3D-EPI blip-up/down acquisition (BUDA) with CAIPI and joint Hankel structured low-rank reconstruction for rapid distortion-free high-resolution T2* mapping

Document status and date:
Published: 01/05/2023

DOI:
10.1002/mrm.29578

Document Version:
Publisher's PDF, also known as Version of record

Document license:
Taverne

Please check the document version of this publication:

• A submitted manuscript is the version of the article upon submission and before peer-review. There can be important differences between the submitted version and the official published version of record. People interested in the research are advised to contact the author for the final version of the publication, or visit the DOI to the publisher's website.
• The final author version and the galley proof are versions of the publication after peer review.
• The final published version features the final layout of the paper including the volume, issue and page numbers.

Link to publication

RESEARCH ARTICLE

Magnetic Resonance in Medicine

3D-EPI blip-up/down acquisition (BUDA) with CAIPI and joint Hankel structured low-rank reconstruction for rapid distortion-free high-resolution T_2^* mapping

Zhifeng Chen[1,2,3,4] | **Congyu Liao**[5] | **Xiaozhi Cao**[5] | **Benedikt A. Poser**[6] |
Zhongbiao Xu[7] | **Wei-Ching Lo**[8] | **Manyi Wen**[9] | **Jaejin Cho**[2,3] |
Qiyuan Tian[2,3] | **Yaohui Wang**[10] | **Yanqiu Feng**[1,11] | **Ling Xia**[12,13] |
Wufan Chen[1] | **Feng Liu**[14] | **Berkin Bilgic**[2,3,15]

[1]School of Biomedical Engineering, Guangdong Provincial Key Laboratory of Medical Image Processing & Guangdong Province Engineering Laboratory for Medical Imaging and Diagnostic Technology, Southern Medical University, Guangzhou, China

[2]Athinoula A. Martinos Center for Biomedical Imaging, Massachusetts General Hospital, Charlestown, Massachusetts, USA

[3]Department of Radiology, Harvard Medical School, Charlestown, Massachusetts, USA

[4]Department of Data Science and AI, Faculty of IT, Monash University, Clayton, Victoria, Australia

[5]Department of Radiology, Stanford University, Stanford, California, USA

[6]Maastricht Brain Imaging Center, Faculty of Psychology and Neuroscience, University of Maastricht, Maastricht, The Netherlands

[7]Department of Radiotherapy, Cancer Center, Guangdong Provincial People's Hospital & Guangdong Academy of Medical Science, Guangzhou, China

[8]Siemens Medical Solutions, Boston, Massachusetts, USA

[9]Department of Chemical Pathology, The Chinese University of Hong Kong, Hong Kong, China

[10]Division of Superconducting Magnet Science and Technology, Institute of Electrical Engineering, Chinese Academy of Sciences, Beijing, China

[11]Guangdong-Hong Kong-Macao Greater Bay Area Center for Brain Science and Brain-Inspired Intelligence & Key Laboratory of Mental Health of the Ministry of Education, Southern Medical University, Guangzhou, China

[12]Department of Biomedical Engineering, Zhejiang University, Hangzhou, China

[13]Research Center for Healthcare Data Science, Zhejiang Lab, Hangzhou, China

[14]School of Information Technology and Electrical Engineering, The University of Queensland, Brisbane, Queensland, Australia

[15]Harvard-MIT Division of Health Sciences and Technology, Massachusetts Institute of Technology, Cambridge, Massachusetts, USA

Correspondence
Yanqiu Feng, School of Biomedical Engineering, Southern Medical University, Guangzhou, China.
Email: foree@163.com

Congyu Liao, Department of Radiology, Stanford University, Stanford, California, USA.
Email: cyliao@stanford.edu

Purpose: This work aims to develop a novel distortion-free 3D-EPI acquisition and image reconstruction technique for fast and robust, high-resolution, whole-brain imaging as well as quantitative T_2^* mapping.

Methods: 3D Blip-up and -down acquisition (3D-BUDA) sequence is designed for both single- and multi-echo 3D gradient recalled echo (GRE)-EPI imaging using multiple shots with blip-up and -down readouts to encode B_0 field map information. Complementary k-space coverage is achieved using controlled aliasing in parallel imaging (CAIPI) sampling across the shots. For image reconstruction, an iterative hard-thresholding algorithm is employed to minimize the cost function that combines field map information informed parallel imaging with the structured low-rank constraint for multi-shot 3D-BUDA data.

Congyu Liao and Yanqiu Feng contributed equally to this work.

Extending 3D-BUDA to multi-echo imaging permits T_2^* mapping. For this, we propose constructing a joint Hankel matrix along both echo and shot dimensions to improve the reconstruction.

Results: Experimental results on in vivo multi-echo data demonstrate that, by performing joint reconstruction along with both echo and shot dimensions, reconstruction accuracy is improved compared to standard 3D-BUDA reconstruction. CAIPI sampling is further shown to enhance image quality. For T_2^* mapping, parameter values from 3D-Joint-CAIPI-BUDA and reference multi-echo GRE are within limits of agreement as quantified by Bland–Altman analysis.

Conclusions: The proposed technique enables rapid 3D distortion-free high-resolution imaging and T_2^* mapping. Specifically, 3D-BUDA enables 1-mm isotropic whole-brain imaging in 22 s at 3T and 9 s on a 7T scanner. The combination of multi-echo 3D-BUDA with CAIPI acquisition and joint reconstruction enables distortion-free whole-brain T_2^* mapping in 47 s at $1.1 \times 1.1 \times 1.0 \, \text{mm}^3$ resolution.

KEYWORDS
CAIPI, distortion-free EPI, joint Hankel low-rank reconstruction, T_2^* mapping, 3D-BUDA

1 | INTRODUCTION

Quantitative MRI has recently gained increased attention in neuroscientific and clinical applications.[1–3] EPI is a rapid encoding technique that has played an essential role in quantitative MRI, including but not limited to functional and diffusion MRI,[4,5] parameter mapping,[1,6,7] and quantitative susceptibility mapping.[8,9]

Despite the high acquisition speed, susceptibility-induced geometric distortions and voxel intensity pile-ups have remained the main drawbacks of EPI.[7,10] To mitigate the geometric distortions present in EPI, a range of correction approaches has been developed.[5,6,11–18] A common approach is to improve the acceleration factor along the phase encoding direction with the aid of parallel imaging to mitigate distortion.[19–23] However, as the acceleration factor increases, the g-factor penalty and under-sampling-associated artifacts may become severe.[19,22,23] To address this, multi-shot EPI acquisition can be employed.[11,13,17] By exploiting multi-shot read-outs, geometric distortion and sub-sampling artifacts caused by high acceleration factors can be simultaneously reduced. Although multi-shot EPI has been beneficial, it suffers from shot-to-shot phase variations which hamper the combination of the shots predominantly in diffusion MRI.[11,14] Hence, shot-to-shot phase correction techniques were introduced to remove phase errors, including navigator-based[15,18,24] and self-navigated approaches.[11,13,14,17] In addition, advanced low-rank approaches utilize structured low-rank in k-space[12,25] or locally low-rank priors in the image domain[13] to help remove shot-to-shot phase variations. However, these approaches mitigate, but do not completely eliminate geometric distortion and voxel pile-ups.

To eliminate distortion, the hybrid-space SENSE approach was proposed for a blip-up/down acquisition scheme to obtain shots with alternating polarities.[16] This enables the estimation of a B_0 field map using, for example, FSL TOPUP.[26] Hybrid-space SENSE incorporates this field map information into the multi-shot SENSE model to obtain distortion-free images.[16,27] More recent work combined field map-informed parallel imaging with Hankel structured low-rank constraint to mitigate remaining phase errors, ghosts, and noise in distortion-free blip-up and -down acquisition (BUDA) EPI.[5,6,28–30] Previous work on BUDA focused on 2D or simultaneous multislice (SMS) encoded imaging,[5,6,28] and did not explore 3D EPI read-outs.[31]

In this work, our contributions include the following:

1. A novel 3D blip-up/down sequence with controlled aliasing in parallel imaging (CAIPI) strategy across shots for better k-space coverage and improved image reconstruction is proposed for single- and multi-echo, multi-shot EPI acquisition;

2. A joint image reconstruction strategy for further correcting phase errors, boosting SNR, and improving the accuracy of BUDA-EPI reconstruction; and

3. Rapid, distortion-free T_2^* mapping from three-echo BUDA imaging.

The rest of this paper is organized as follows: In the next section, sequence diagrams of 3D blip-up and -down acquisition (3D-BUDA) single- and multi-echo acquisitions are provided, and hybrid-space SENSE and standard Hankel structured low-rank scheme are introduced; subsequently, the new joint BUDA image reconstruction among both echo/contrast and shot dimensions are proposed; lastly, reconstruction evaluation criteria are listed. Section 3 demonstrates the performance of the proposed scheme in vivo. Section 4 discusses the advantages and limitations of the proposed method; future work is also considered. The last section draws conclusions. Part of this work was published as abstracts in the proceedings of the International Society for Magnetic Resonance in Medicine, 2020[32] and 2022.[33]

2 | METHODS

2.1 | 3D-BUDA acquisition

Figure 1 shows the sequence diagram of the 3D-BUDA sequence and the k-space trajectory. Multi-echo EPI data were acquired with interleaved EPI shots of reversed polarity along the phase-encoding direction, creating opposing distortions to obtain B_0 field maps for model-based distortion correction.[16] A three-echo navigator was included

for ghost correction (not shown).[34] A Siemens product excitation pulse with optimized amplitude modulation was used to suppress ripples, with an radiofrequency duration of 2.56 ms. Using high $R_{inplane}$ acceleration per shot, three echoes with adequate TEs for T_2^* mapping could fit within a single pulse repetition time (TR).

To obtain FOV-matched coil sensitivity maps, a 3D low-resolution FLASH acquisition was included along with the 3D-BUDA sequence.

While the number of echoes can be adjusted flexibly, we used three echoes for T_2^* mapping, as detailed later. Blip-up/down phase encodings were implemented for each echo (yellow and green blips in phase encoding gradient, respectively). Different shots with staggered k-space trajectories along k_y and k_z dimensions were acquired using additional gradients in the pre-phasing part of G_{PE} and G_z for each echo, respectively. For different shots with different k_y shifts, the echo-train was delayed according to.[35]

To reduce the g-factor penalty of the highly accelerated data and improve the conditioning of the reconstruction, different CAIPI shifts[36–38] in the k_y-k_z dimension were also employed in different blip-up/down shots.

2.2 | Image reconstruction

Coil sensitivity maps were estimated using ESPIRiT[39] from the FOV-matched low-resolution 3D FLASH reference data.
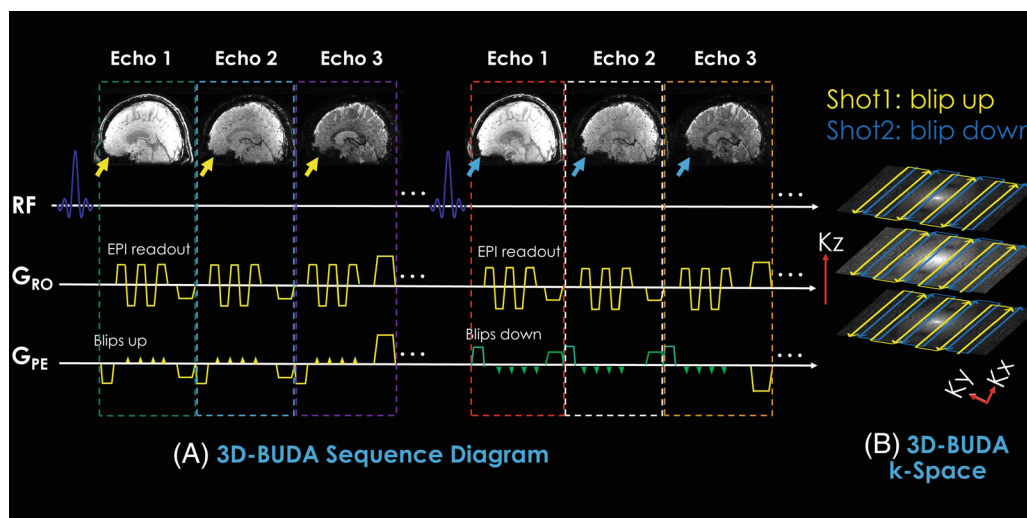
FIGURE 1 The sequence diagram of the 3D blip-up and -down acquisition-EPI (3D-BUDA-EPI) for multi-echo imaging (A) and k-space trajectory (B). 3D slab-selective EPI data were acquired using a complementary blip-up /down acquisitions multi-shot encoding with water excitation. Blip-up /down sampling was implemented for each echo (see yellow and green blips in phase encoding gradient), followed by a rewinder gradient before the next echo. All blip-up shots with all echoes were acquired first, then blip-down shots

2.2.1 | Hankel low-rank reconstruction for single-echo 3D-BUDA

3D-BUDA reconstruction incorporates B_0 forward-modeling into structured low-rank reconstruction to enable distortion-free EPI, as shown in Figure S1:

$$\operatorname*{argmin}_{I} \sum_{t} \|M_t F_t E(C \odot I_t) - d_t\|_F^2, \quad s.t.\mathrm{rank}(\mathcal{H}(I)) = r \tag{1}$$

Where t represents the shot number index, M is the sampling mask, F_t is the discrete Fourier transform operator, and E is the B_0 field map generated by *TOPUP* using FSL (http://fsl.fmrib.ox.ac.uk/fsl).[26] C is the coil sensitivity map, I denotes the to-be-restored images, the $\odot$ symbol denotes the Hadamard (or elementwise) product between two matrixes, and d_t represents the acquired under-sampled k-space data of tth shot. $\mathcal{H}(I)$ represents the Hankel low-rank matrix which enforces low-rankness across different shots, and r is the target rank. Herein, the Hankel matrix was constructed by consecutively using $9 \times 9 \times 9$ neighborhood points in k-space from each shot as a Hankel-block and then concatenating them in the column dimension. A fast iterative algorithm is used to solve this equation. The RMS error (RMSE) of less than 0.1% between consecutive iterations was used to check for convergence.

2.2.2 | Joint Hankel low-rank image reconstruction for multi-echo 3D-BUDA

We further improve the performance of structured low-rank reconstruction by utilizing the echo dimension, as shown in Figure 2:

$$\operatorname*{argmin}_{I} \sum_{t,n} \|M_{t,n} F_{t,n} E(C \odot I_{t,n}) - d_{t,n}\|_F^2,$$
$$s.t.\mathrm{rank}(\mathcal{H}(I)) = \gamma \tag{2}$$

Where t is the shot index, and n represents the echo index. Other symbols and variables are the same as the previous Eq. (1), whereas the $\mathcal{H}(I)$ here indicates the new joint Hankel matrix.

The proposed joint reconstruction constructs a Hankel matrix along both shot and echo dimensions for multi-echo 3D-BUDA data. It enforces local k-space neighborhoods, extended across all echoes/-contrasts in the shot dimension, to have structured low-rankness property. This is expected to take better advantage of the similarities across multiple images along the echo dimension. The neighborhood size for a Hankel-block is now $9 \times 9 \times 9 \times n$ (n: echo number). Therefore, the new size of the block-Hankel matrix is $((N_{\mathrm{FE}} - m + 1) \times (N_{\mathrm{PE}} - m + 1) \times (N_z - m + 1)) \times (m^3 \times n)$ (N_{FE}: number of the sampled points in frequency encoding dimension, N_{PE}: number of the sampled points in phase encoding dimension, N_z: number of k_z partitions, m: kernel size), which is constructed by consecutively using $9 \times 9 \times 9 \times n$ neighborhood points as a Hankel-block and then concatenating them in the column dimension. The convergence condition is the same as above.

2.2.3 | T_2^* mapping

Quantitative T_2^* ($=1/R_2^*$) mapping was performed using variable projection (VARPRO)[40] on the reconstructed volumes with a dictionary comprising signal evolution
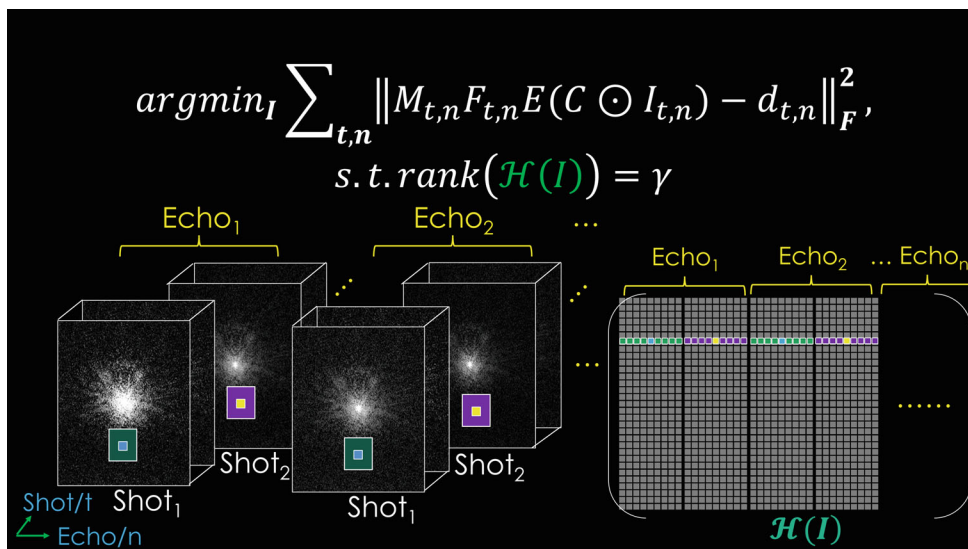

FIGURE 2 The proposed 3D joint-blip-up and -down acquisition image reconstruction framework for multi-echo multi-shot gradient recalled echo (GRE) -EPI data. The new Hankel matrix is formed for joint image reconstruction using both echo and shot neighborhood information of the GRE-EPI dataset

curves of T_2^* from 1 to 125 ms with a step size of 1 ms, 126 to 300 ms with a step size of 3 ms. A reference multi-echo GRE sequence was used as the gold standard T_2^* mapping method.

2.3 | Experiments design

In vivo experiments were performed under approval of the Institutional Review Board on six healthy volunteers.

2.3.1 | Single-echo 3D-BUDA for fast whole-brain imaging at 3T and 7T

Data were acquired on a 3T MR Scanner (Magnetom Trio System; Siemens Healthineers, Erlangen, Germany) equipped with a 32-channel head coil. The gradient performance was a gradient strength of 45 mT/m and a slew rate of 200 T/m/s. The imaging parameters for four-shot and two-shot 3D-BUDA included: $R_{inplane} = 4$ and $R_z = 1$ or 2, FOV $224 \times 224 \times 128$ mm^3, TR/TE $= 72/36$ ms, resolution $1 \times 1 \times 1$ mm^3, and flip angle 16° (Ernst angle). The effective acceleration factor is $R_{effective} = 2$ and the total acquisition times (TA) are 22 s in all cases, including a FLASH low-resolution pre-scan for coil sensitivity estimation. Detailed parameters can be found in Table 1.

Additional in vivo data were also acquired on a 7T MR Magnetom Scanner (Siemens Healthineers, Erlangen, Germany) using a 32-channel head coil array. The gradient performance was a gradient strength of 70 mT/m and a slew rate of 200 T/m/s. The imaging parameters for two-shot 3D-BUDA included: $R_{inplane} = 5$ and $R_z = 1$ or 2, FOV $224 \times 224 \times 128$ mm^3, TR/TE $= 50/25$ ms, the spatial resolution of $1 \times 1 \times 1$ mm^3, and flip angle 16°. The effective acceleration factors are $R_{effective} = 2.5$ and 5, and TA $= 16$ s ($R_z = 1$) and TA $= 9$ s ($R_z = 2$), respectively. More parameters can be found in Table 2.

2.3.2 | Multi-echo 3D-BUDA for rapid whole-brain T_2^* mapping at 3T

For T_2^* mapping, multi-echo, multi-shot in vivo imaging experiments were performed on the same 3T scanner with the standard 32-element head coil. Imaging parameters for eight-shot and four-shot 3D-BUDA included: $R_{inplane} = 8$ and $R_z = 1$ or 2, FOV $220 \times 220 \times 128$ mm^3, TR $= 86$ ms, TE $= \{18, 43.17, 68.34\}$ ms, and flip angle 19°, resulting in a spatial resolution of $1.1 \times 1.1 \times 1.0$ mm^3. The effective acceleration factor is $R_{effective} = 2$, and TA $= 47$ s in all cases. Detailed information of parameters can be found in Table 3.

TABLE 1 The sequence parameters for in vivo single-echo 3D-BUDA experiments @ 3 T

Acquisition parameters	Single-echo 3D-BUDA @ 3T (Magnetom Trio system)			
FOV (mm^3)	$224 \times 224 \times 128$	$224 \times 224 \times 128$	$224 \times 224 \times 128$	$224 \times 224 \times 128$
Resolution (mm^3)	$1 \times 1 \times 1$	$1 \times 1 \times 1$	$1 \times 1 \times 1$	$1 \times 1 \times 1$
TR (ms)	72	72	72	72
TE (ms)	36	36	36	36
Flip angle (°)	16	16	16	16
EPI factor	128	128	128	128
No. of coil elements	32	32	32	32
No. of shots (N_s)	4	4	4	2
$R_{inplane}$	4	4	4	4
R_z	1	2	2	1
CAIPI (Y or N)	N	Y, z-shift = 1	N	N
BW$_x$ (Hz/pixel)	1116	1116	1116	1116
BW$_y$ (Hz/pixel)	16.85	16.85	16.85	16.85
ACS	32×32	32×32	32×32	32×32
$R_{effective}$ ($R_{inplane} \times R_z / N_s$)	1	2	2	2
Acquisition time (s)	41	22	22	22
Figure	Figure 3A	Figure 3B	Figure 3C	Figures 3D,E and 4

Abbreviation: 3D-BUDA, 3D-blip-up and -down acquisition; ACS, autocalibration scan (y × z matrix); BW, bandwidth; CAIPI (Y or N), CAIPIRINHA (Yes or No).

TABLE 2 Sequence parameters for in vivo single-echo 3D-BUDA experiments @ 7T

Acquisition parameters	Single-echo 3D-BUDA @ 7T (Magnetom system)	
FOV (mm^3)	$224 \times 224 \times 128$	$224 \times 224 \times 128$
Resolution (mm^3)	$1 \times 1 \times 1$	$1 \times 1 \times 1$
TR (ms)	50	50
TE (ms)	25	25
Flip angle (°)	16	16
EPI factor	128	128
No. of coil elements	32	32
No. of shots (N_s)	2	2
$R_{inplane}$	5	5
R_z	1	2
BW$_x$ (Hz/pixel)	1313	1313
BW$_y$ (Hz/pixel)	25.08	25.08
ACS	32×32	32×32
$R_{effective}$ ($R_{inplane} \times R_z / N_s$)	2.5	5
Acquisition time (s)	16	9
Figure	Figure S2	Figure 5

Abbreviation: 3D-BUDA, 3D-blip-up and -down acquisition; ACS, autocalibration scan (y × z matrix); BW, bandwidth; CAIPI (*Y* or *N*), CAIPIRINHA (Yes or No).

TABLE 3 The sequence parameters for in vivo multi-echo 3D-BUDA experiments @ 3T

Acquisition parameters	Multi-echo 3D-BUDA @ 3T (Magnetom Trio system)			
FOV (mm^3)	$220 \times 220 \times 128$	$220 \times 220 \times 128$	$220 \times 220 \times 128$	$220 \times 220 \times 128$
Resolution (mm^3)	$1.1 \times 1.1 \times 1$	$1.1 \times 1.1 \times 1$	$1.1 \times 1.1 \times 1$	$1.1 \times 1.1 \times 1$
TR (ms)	86	86	86	86
TE (ms)	{18, 43.17, 68.34}	{18, 43.17, 68.34}	{18, 43.17, 68.34}	{18, 43.17, 68.34}
Flip angle (°)	19	19	19	19
EPI factor	128	128	128	128
No. of coil elements	32	32	32	32
No. of shots (N_s)	8	8	8	4
$R_{inplane}$	8	8	8	8
R_z	1	2	2	1
CAIPI (*Y or N*)	N	Y, z-shift =1	N	N
BW$_x$ (Hz/pixel)	1302	1302	1302	1302
BW$_y$ (Hz/pixel)	42.95	42.95	42.95	42.95
ACS	32×32	32×32	32×32	32×32
$R_{effective}$ ($R_{inplane} \times R_z / N_s$)	1	2	2	2
Acquisition time (s)	92	47	47	47
Figure	-	Figure 6E,F	Figure 6C,D	Figure 6A,B

Abbreviation: 3D-BUDA, 3D-blip-up and -down acquisition; ACS, autocalibration scan (y × z matrix); BW, bandwidth; CAIPI (*Y* or *N*), CAIPIRINHA (Yes or No).

To generate a reference T_2^* map, standard multi-echo 3D-GRE imaging experiments were also performed. The relevant imaging parameters included: FOV $220 \times 220 \times 128$ mm^3, TR = 86 ms, TE = {6, 18, 30, 43.17, 55, 68.34} ms, and flip angle 19°, resulting in a spatial resolution of $1.1 \times 1.1 \times 1.0$ mm^3. The total acquisition time was ~35 min.

All image reconstructions were implemented in MATLAB (R2020b; the Mathworks, Inc., Natick, MA, USA) for off-line reconstruction using a Linux (CentOS) workstation with 48-Core Intel(R) Xeon(R) Gold 6248R CPU @ 3.00GHz and 512 GB of memory.

Parallel computing was also performed for all 3D-BUDA image reconstructions in MATLAB using the *parfor* operator by employing 48 cores. In this way, the reconstruction procedure was sped up, and it takes ~575 s to reconstruct whole-brain, single-echo 3D-BUDA data.

2.4 | Evaluation of accuracy

For image quality assessment, RMSE and Structure Similarity[41] were used with a fully-sampled reference.

In this work, we have used a distortion-free "fully sampled" BUDA-reconstructed image as a reference ($R_{effective} = 1$). For the single-echo experiment at 3T, the four-shot reference was sampled at $R_{inplane} \times R_z = 4 \times 1$ acceleration per shot. For the multi-echo experiment, the eight-shot reference was sampled at $R_{inplane} \times R_z = 8 \times 1$ acceleration per shot.

For T_2^* mapping evaluation, Bland–Altman analysis[42] was used. Several regions of interest were manually selected. Reference T_2^* maps were obtained from a standard 3D GRE multi-echo sequence.

3 | RESULTS

3.1 | 3D-BUDA GRE-EPI for fast whole-brain imaging at 3T

Figures 3 and 4 show the reconstruction results of single-echo 3D-BUDA data at 3T. In Figure 3, we compare different sampling schemes for 3D-BUDA imaging. As shown in Figure 3B–D, with matching scan time, four-shot $R_z = 2$ with and without CAIPI sampling generates better reconstruction accuracy than two-shot $R_z = 1$ case (RMSE: 3.11% without CAIPI shift and 3.04% with CAIPI shift vs. 7.22%), while the data with the CAIPI sampling has lower RMSE (3.04% vs. 3.11%) under the same
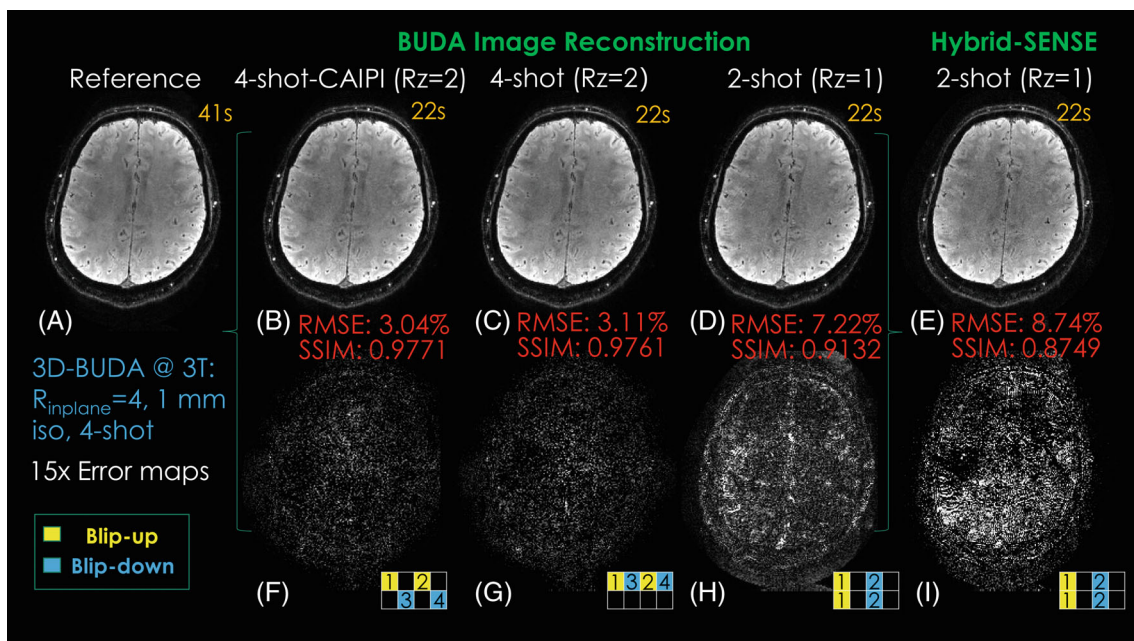

FIGURE 3 Comparison of reconstructed results and error maps of different time-matched acquisition schemes and reconstruction approaches. (A) Reference image by fully-sampled 3D-blip-up and -down acquisition (3D-BUDA) image reconstruction. (B) Four-shot $R_z = 2$ CAIPI acquisition with 3D-BUDA reconstruction result (two blip-up shots and two blip-down shots). (C) Four-shot $R_z = 2$ conventional acquisition with 3D-BUDA image reconstruction (two blip-up shots and two blip-down shots). (D) Two-shot $R_z = 1$ acquisition with 3D-BUDA image reconstruction (one blip-up shot and one blip-down shot). (E) Two-shot $R_z = 1$ acquisition with Hybrid-space SENSE image reconstruction (one blip-up shot and one blip-down shot). (F–I) are the corresponding difference maps. The numbers in the sampling mask represent the acquisition order of the shots
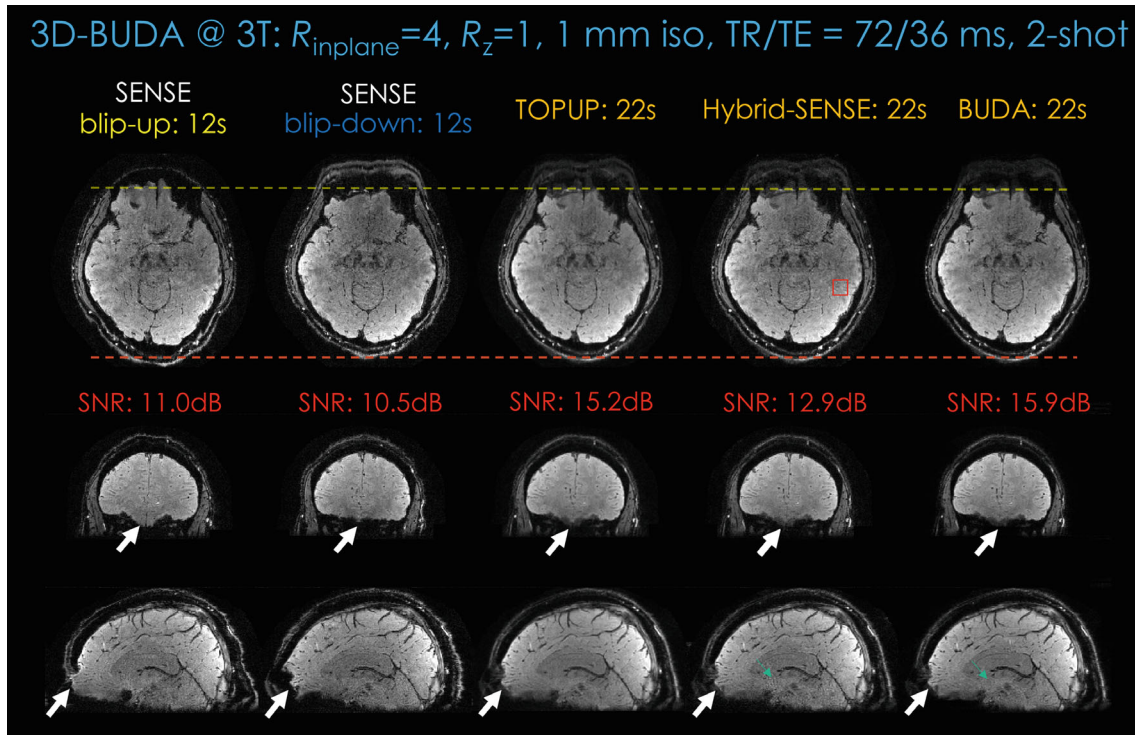
FIGURE 4 Comparison of different approaches (SENSE, TOPUP, Hybrid-space SENSE, and 3D-BUDA [3D-blip-up and -down acquisition]) on image quality and distortion-correction effect for the same two-shot GRE-EPI BUDA dataset from a 3T scanner. First column: blip-up EPI SENSE results. Second column: blip-down EPI SENSE results. Third column: TOPUP results. Fourth column: hybrid-space SENSE results. Last column: the 3D-BUDA image reconstruction. Three rows are the three planes of 3D imaging. In this dataset, $R_{inplane} \times R_z = 4 \times 1$. The total acquisition times of blip-up EPI, blip-down EPI, TOPUP, Hybrid-space SENSE, and 3D-BUDA are 12, 12, 22, 22, and 22 s, respectively. A 2-s FOV-matched FLASH low-resolution scan for coil sensitivity map is included in these experiments. Local SNR values are calculated for all the approaches. Region of interest is drawn in the Hybrid-space SENSE result in axial view (see red square in the first row)

acceleration factor. All the Hankel structured low-rank BUDA image reconstruction have better RMSE than Hybrid-space SENSE (8.74% > 7.22% > 3.11% > 3.04%). Structure Similarity values were also consistent with RMSEs.

Conventional SENSE, TOPUP, hybrid-space SENSE, and the proposed 3D-BUDA results for the same two-shot data are shown in Figure 4. The distortion correction effect can be observed (white arrows and the two dotted lines). TOPUP, hybrid-space SENSE, and BUDA reconstruction can all correct distortion due to the incorporated self-estimated field map information. The results of TOPUP are not much inferior when compared to the Hybrid-space SENSE and the BUDA reconstruction. However, TOPUP results seem to suffer from blurring, ostensibly due to the incorporated image interpolation step. At the same time, BUDA can further remove the remaining noise and phase errors in hybrid-space SENSE (the green arrows in Figure 4). The local-regions of interest SNR estimates in this figure also support an SNR benefit of BUDA. In addition, phase images can also be generated by the proposed BUDA image reconstruction, as shown in Figure S2.

Comparing the reconstruction results with the same scan time in Figure 3, it can be seen that the proposed CAIPI sampling with Hankel low-rank constraint provides the best accuracy. When comparing different sampling patterns with the same Hankel low-rank constraint reconstruction, even the distribution of k_y-k_z acceleration is better than simple k_y acceleration for the same scan time.

3.2 | 3D-BUDA GRE-EPI for fast whole-brain imaging at 7T

Figures 5 and S3 demonstrate the reconstruction results at 7T with $R_{inplane} = 5$-fold acceleration using two shots. Reconstructions using SENSE, TOPUP, hybrid-space SENSE, and BUDA are shown. The distortion correction effect can be seen from the two dotted lines. TOPUP results still suffer from some blurring when compared with hybrid-space SENSE and BUDA. Phase errors and some remaining ghosts/artifacts were further mitigated in BUDA compared to hybrid-space SENSE. In addition, the area showing phase errors in Figure 5 ($R_{inplane} \times R_z = 5 \times 2$)
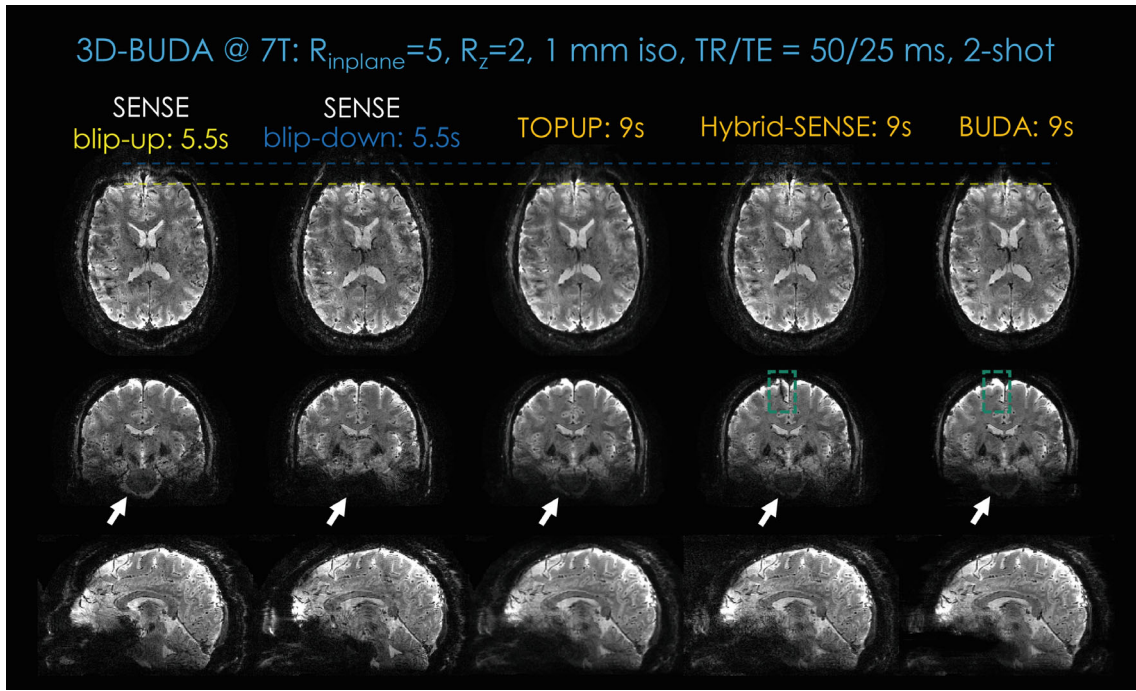
FIGURE 5 Comparison of different approaches (SENSE, TOPUP, Hybrid-space SENSE, and 3D-BUDA [3D-blip-up and -down acquisition]) on image quality and distortion-correction effect for the same two-shot BUDA at 7T. First column: blip-up SENSE results. Second column: blip-down SENSE results. Third column: TOPUP results. Fourth column: hybrid-space SENSE results. Last column: the 3D-BUDA image reconstruction results. Three rows are the three planes of 3D imaging. In this dataset, $R_{\text{inplane}} \times R_z = 5 \times 2$. The total acquisition times of blip-up EPI, blip-down EPI, TOPUP, Hybrid-space SENSE, and 3D-BUDA are 5.5, 5.5, 9, 9, and 9 s, respectively. A 2-s FOV-matched FLASH low-resolution scan for coil sensitivity map is counted in these acquisitions
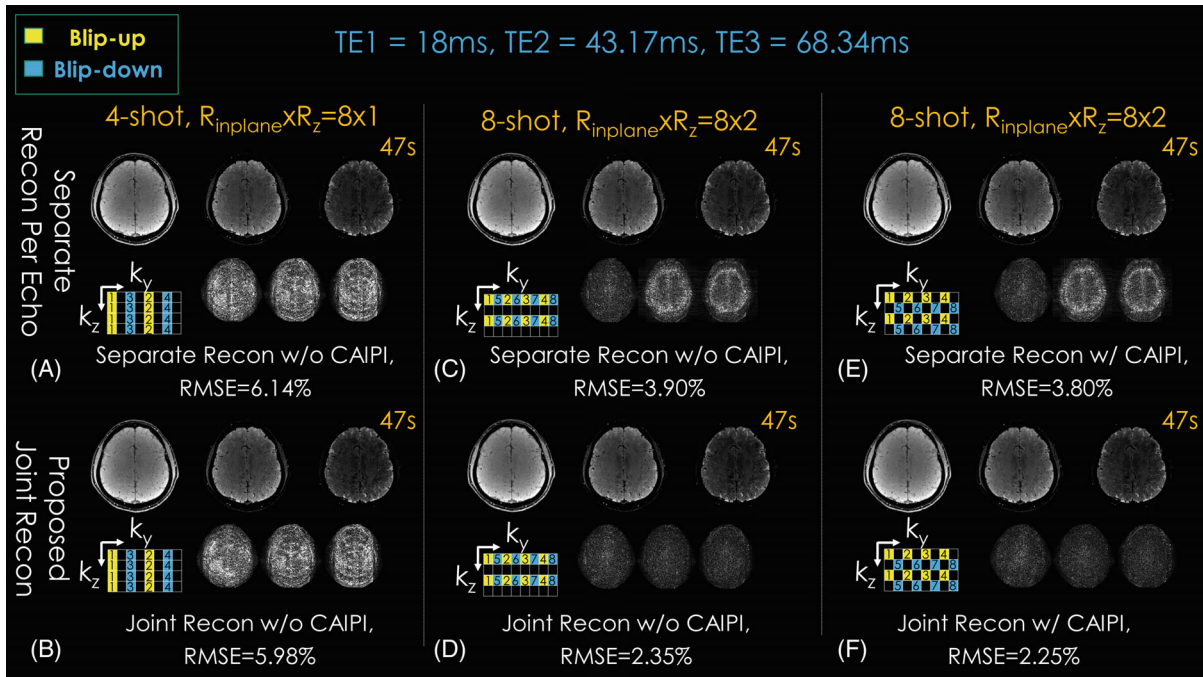

FIGURE 6 Comparison of different approaches with different sampling patterns (lower left corner of each subpart) on image quality for 3D-blip-up and -down acquisition dataset with the same sampling amount (total acquisition time: 47 s). The difference maps were located in the lower-right corner of each subpart. First column: conventional four-shot $R_z = 1$ without and with joint structured low-rank reconstruction. Second column: conventional eight-shot sampling without and with joint structured low-rank reconstruction. Third column: eight-shot with CAIPIRINHA sampling without and with joint structured low-rank reconstruction. Three columns in each subpart are the three echoes of 3D-blip-up and -down acquisition imaging. The numbers in the sampling mask represent the acquisition order of the shots
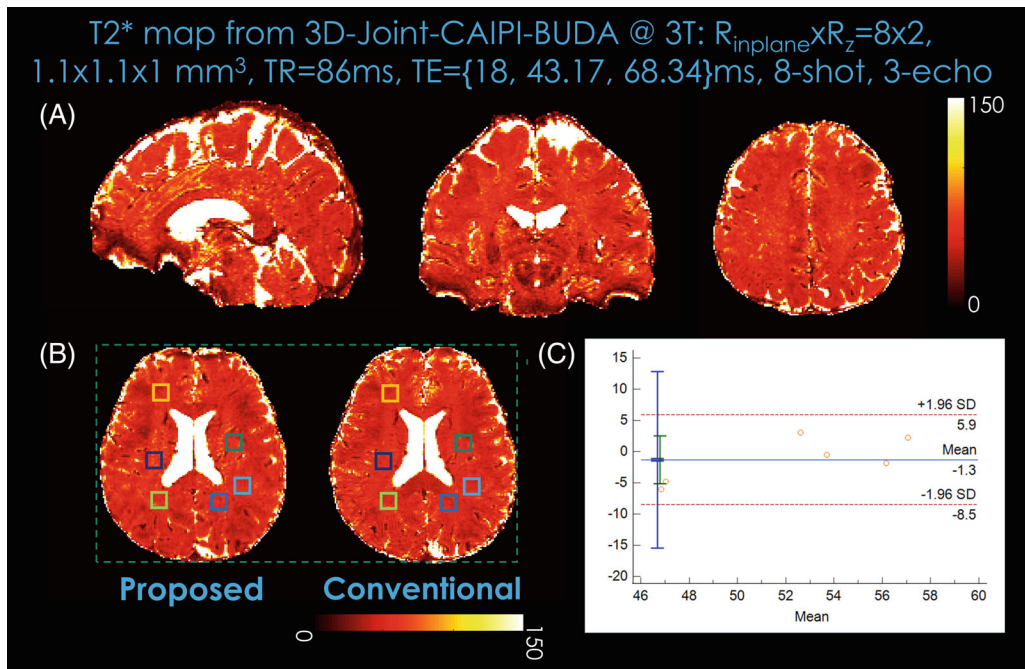
FIGURE 7 Comparison of the Bland–Altman plots displaying the mean and difference of T_2^* mapping generated by 3D-Joint-CAIPI-BUDA image reconstruction and standard multi-echo GRE. (A) T_2^* mapping generated by 3D-joint-CAIPI-BUDA (eight-shot, $R_{inplane} \times R_z = 8 \times 2$). (B) Selected regions of interest for Bland–Altman plots. (C) 3D-Joint-CAIPI-BUDA ($R_{inplane} \times R_z = 8 \times 2$, eight-shot) versus standard multi-echo GRE (mean: GRE = 51.58 vs. 3D-Joint-CAIPI-BUDA = 52.88). BUDA, blip-up and -down acquisition; CAIPI, CAIPIRINHA

was restored in the 3D-BUDA reconstruction (green dotted boxes).

3.3 | 3D-BUDA GRE-EPI for fast whole-brain T_2^* mapping

Figure 6 shows the multi-echo, multi-shot 3D-BUDA acquisition results at $R_{inplane} = 8$. The absolute difference maps were also displayed between reference and reconstruction results. Two time-matched acceleration strategies are considered: Sampling eight-shots at $R_z = 2$-fold partition acceleration and four-shots at $R_z = 1$. Both joint multi-echo and separate reconstructions for each echo are performed.

When echoes are separately reconstructed, $R_{inplane} \times R_z = 8 \times 2$ case using eight-shot has higher reconstruction accuracy (3.90% RMSE) than $R_{inplane} \times R_z = 8 \times 1$ with four-shot (6.14%), due to more evenly distributed k_y-k_z sampling pattern. In the $R_{inplane} = 8$ case, having acquired eight-shot also permitted better B_0 estimation using interim four-shot blip-up and four-shot blip-down reconstructions in *Topup* (see Figure S4), which were "effectively" $R_{inplane} \times R_z = 2 \times 2$-fold accelerated and could be readily reconstructed using SENSE.

Joint reconstruction with CAIPI sampling across echoes/shots further improved these results, where eight-shot $R_{inplane} \times R_z = 8 \times 2$ with CAIPI shift yielded 2.25%, and four-shot $R_{inplane} \times R_z = 8 \times 1$ had 5.98% RMSE. Thus, the proposed joint multi-contrast reconstruction with CAIPI shift provided more than 2.5-fold improvement over separate reconstructions without CAIPI shift, and ~1.7-fold improvement over separate reconstructions with CAIPI shift (3.8% RMSE).

For T_2^* mapping, Figure 7 shows the Bland–Altman analysis of the proposed 3D-BUDA and standard multi-echo 3D-GRE. The Bland–Altman plots show the mean and difference for the regions of interests (see squares in Figure 7B) of T_2^* values. The Bland–Altman analysis results demonstrated that the T_2^* maps estimated by the 3D-CAIPI-BUDA sampling pattern with joint reconstruction and standard multi-echo GRE are within the limits of agreement, although minor biases (−1.3 ms) exist.

4 | DISCUSSION

In this work, we proposed a 3D blip-up and blip-down sequence with CAIPI sampling for rapid single- and/or

multi-contrast high-resolution T_2^*-weighted image acquisition. Contributions of this work include: (1) 3D-BUDA sequence with CAIPI sampling along shot dimensions for improved image reconstruction is proposed for rapid, high-resolution, whole-brain T_2^*-weighted imaging; (2) extension of this to multi-echo sampling and distortion-free T_2^* mapping; and (3) exploring joint Hankel regularization along the additional echo dimension in multi-echo acquisitions, thus leading to more accurate reconstruction than separate Hankel-constrained reconstructions per echo.

4.1 | Improved sampling pattern in 3D-BUDA

As explored previously, CAIPI distributes the under-sampling more evenly in k-space and helps improve image quality.[36–38] Herein, eight-shot, $R_z = 2$ case can generate better results than the time-matched, four-shot, and $R_z = 1$ case (Figure 6). Due to more evenly distributed k-space sampling locations, the CAIPI sampling pattern has lower RMSE and higher accuracy than the non-CAIPI case.

To provide high-fidelity B_0 maps for 3D-BUDA reconstruction, initial blip-up and -down SENSE reconstruction results must be made at moderate acceleration levels. This was made possible by using eight shots at $R_{inplane} \times R_z = 8 \times 2$. The alternative approach of four-shot, $R_{inplane} \times R_z = 8 \times 1$ is less favorable, as can be seen in the Results section(Figure 6), since each blip-up and -down reconstruction will be made at $R_{inplane} \times R_z = 4 \times 1$. As such, joint image reconstruction combined with eight-shot CAIPI acquisition with $R_z = 2$ partition acceleration was proposed for robust T_2^* mapping.

4.2 | Separate versus joint BUDA reconstruction

Herein, joint reconstruction among echo dimensions was proposed to enhance the image reconstruction accuracy of multi-echo 3D-BUDA. The proposed joint multi-echo Hankel low-rank reconstruction for 3D-EPI BUDA has a minor difference from the previous (joint) reconstructions for 2D (gSlider) EPI.[6] In the previous joint reconstruction, the block Hankel matrix is constructed by grouping two successive TEs where one image is acquired with blip-up and the other with blip-down encoding. In the current proposal, all echoes and shots are jointly considered during the Hankel low-rank reconstruction. It stacks data from all contrasts in the shot dimension and enforces local k-space neighborhoods, now extended across all echoes/contrasts in the shot dimension, to have

low-rank property during the reconstruction. Leveraging similarities between echoes helped improve the image quality of multi-echo 3D-BUDA reconstruction, leading to more accurate T_2^* imaging.

4.3 | Parameter selection

The target rank was empirically selected for each experiment and was different for each imaging experiment. In our single-echo 3T experiments in Figure 3, the target rank r is set to 1.5. In 7T results, this parameter is set to 1.25. In multi-echo joint reconstruction, the target rank is set to 4.5.

4.4 | Limitations and extensions

For T_2^* maps generated by multi-echo imaging, the number of echoes presents a tradeoff between imaging speed and the accuracy of T_2^* mapping. If the number of echoes is further decreased, the imaging time will be shortened at the cost of the accuracy of T_2^* mapping. On the contrary, if the number of echoes increases, the scan time will be prolonged with potentially more accurate T_2^* mapping. For the standard T_2^* map calculation, all six TEs of the fully sampled multi-echo GRE were used in this work. Still, this protocol was not optimized but matched to the 3D-BUDA acquisition with respect to the main contrast-encoding parameters (TE/TR/flip angle).

To insert three echoes with adequate TEs for quantitative imaging, the minimum TE (first TE) needed to be made as small as possible. Thus, high in-plane acceleration with the multi-shot acquisition was exploited. Due to the faster T_2^* decay at 7T, higher in-plane acceleration factors may be needed to permit T_2^* mapping using 3D-BUDA.

In this work, a 7T signal boost permits partition acceleration as the intrinsic SNR loss is accounted for. However, there are still some remaining artifacts in the 7T BUDA results (see Figures 5 and S3); these might come from physiological noise (including cardiac, respiratory motion, and the flow of cerebrospinal fluid), which adversely affected the image quality. At 3T, the impact of physiologic noise and intravoxel dephasing can also be observed, for example, in T_2^* maps presented in Figure 7.

The specific absorption rate (SAR) issue is critical in 7T imaging experiments, which is commonly related to, for example, flip angle, slice thickness, radiofrequency duration, and transmission voltage.[43–45] In this study, we use a low flip angle, and slab-selective radiofrequency pulse, SAR limitations were not observed in the 7T experiments.

In terms of computation time, current BUDA-based image reconstruction requires initial SENSE

reconstruction and field map estimation using *Topup*, which prolongs the total reconstruction time.

Currently, our sequence can only acquire echo-dependent sampling data; that is, the CAIPI sampling pattern is fixed for each echo. An echo-independent acquisition strategy may be more flexible. With staggered sampling across both shot and echo dimensions, the g-factor and SNR benefit may be further improved. Further gains in image quality can be obtained using novel CAIPI sampling,[46–48] virtual coil concept,[49,50] and artificial sparsity-based image reconstruction.[23,51,52] For instance, skipped-CAIPI sampling with increased protocol flexibility for high-resolution EPI[47] can be applied for SNR and efficiency benefit in future 3D-BUDA. Shot-selective 2D CAIPIRINHA can also be exploited to further push the limits of acceleration and resolution.[46] Furthermore, a clustering-based motion correction approach can be introduced to improve motion robustness.[15] Deep learning approaches can also be investigated to enhance image quality and enable higher accelerations.[53–59]

5 | CONCLUSIONS

The proposed 3D-BUDA combines multi-shot acquisition using alternating polarities with a B_0-informed and structured low-rank regularized reconstruction to boost SNR and eliminate distortions. This permits the acquisition of distortion-free whole-brain data with high quality in 22 s on 3T and 9 s at 7T at 1 mm isotropic resolution on the Siemens systems available in this work. In multi-echo imaging, the proposed joint Hankel structured low-rank reconstruction along both shot and echo dimensions further improves the reconstruction. This enables distortion-free T_2^* mapping with whole-brain coverage at the resolution of $1.1 \times 1.1 \times 1.0\,mm^3$ in 47 s.

CONFLICT OF INTEREST

Wei-Ching Lo is a Staff Scientist at Siemens Healthineers, USA.

DATA AVAILABILITY STATEMENT

All the sample data were performed according to procedures approved by the local Internal Review Board after obtaining informed suitable written consents. All the 3T data, as well as the 7T data, will be made available on request, via a request to the corresponding author. Two exemplar 3D-BUDA data are made available at https://zenodo.org/record/7412718#.Y7OMSOxByX2.

The main image reconstruction code that supports the findings is available at https://github.com/zjuczf168/zjuczf168.

ORCID

Zhifeng Chen https://orcid.org/0000-0001-7824-373X
Congyu Liao https://orcid.org/0000-0003-2270-276X
Benedikt A. Poser https://orcid.org/0000-0001-8190-4367
Jaejin Cho https://orcid.org/0000-0001-5672-6765
Qiyuan Tian https://orcid.org/0000-0002-8350-5295
Yaohui Wang https://orcid.org/0000-0001-6434-5356
Yanqiu Feng https://orcid.org/0000-0002-2807-5974
Berkin Bilgic https://orcid.org/0000-0002-9080-7865

REFERENCES

1. Larsen B, Olafsson V, Calabro F, et al. Maturation of the human striatal dopamine system revealed by PET and quantitative MRI. *Nat Commun*. 2020;11:1-10.
2. Gracien RM, Maiworm M, Brüche N, et al. How stable is quantitative MRI? – assessment of intra- and inter-scanner-model reproducibility using identical acquisition sequences and data analysis programs. *Neuroimage*. 2020;207:1-11.
3. van Wijnen A, Petrov F, Maiworm M, et al. Cortical quantitative MRI parameters are related to the cognitive status in patients with relapsing-remitting multiple sclerosis. *Eur Radiol*. 2020;30:1045-1053.
4. Bandettini PA. Twenty years of functional MRI: the science and the stories. *Neuroimage*. 2012;62:575-588.
5. Liao C, Cao X, Cho J, Zhang Z, Setsompop K, Bilgic B. Highly efficient MRI through multi-shot echo planar imaging. *Wavelets and Sparsity XVIII*. Vol 11138. SPIE; 2019:43.
6. Cao X, Wang K, Liao C, et al. Efficient T2 mapping with blip-up/down EPI and gSlider-SMS (T2-BUDA-gSlider). *Magn Reson Med*. 2021;86:2064-2075.
7. Dierkes T, Neeb H, Shah NJ. Distortion correction in echo-planar imaging and quantitative T2* mapping. *Int Congr Ser*. 2004;1265:181-185.
8. Langkammer C, Bredies K, Poser BA, et al. Fast quantitative susceptibility mapping using 3D EPI and total generalized variation. *Neuroimage*. 2015;111:622-630.
9. Wang F, Dong Z, Reese TG, et al. Echo planar time-resolved imaging (EPTI). *Magn Reson Med*. 2019;81:3599-3615.

10. Ardekani S, Sinha U. Geometric distortion correction of high-resolution 3 T diffusion tensor brain images. *Magn Reson Med*. 2005;54:1163-1171.

11. Chen-kuei N, Guidon A, Chang HC, Song AW. A robust multi-shot scan strategy for high-resolution diffusion weighted MRI enabled by multiplexed sensitivity-encoding (MUSE). *Neuroimage*. 2013;72:41-47.

12. Mani M, Jacob M, Kelley D, Magnotta V. Multi-shot sensitivity-encoded diffusion data recovery using structured low-rank matrix completion (MUSSELS). *Magn Reson Med*. 2017;78:494-507.

13. Hu Y, Levine EG, Tian Q, et al. Motion-robust reconstruction of multishot diffusion-weighted images without phase estimation through locally low-rank regularization. *Magn Reson Med*. 2019;81:1181-1190.

14. Chu ML, Chang HC, Chung HW, Truong TK, Bashir MR, Chen NK. POCS-based reconstruction of multiplexed sensitivity encoded MRI (POCSMUSE): A general algorithm for reducing motion-related artifacts. *Magn Reson Med*. 2015;74:1336-1348.

15. Xu Z, Huang F, Wu Z, et al. Technical note: clustering-based motion compensation scheme for multishot diffusion tensor imaging. *Med Phys*. 2018;45:5515-5524.

16. Zahneisen B, Aksoy M, Maclaren J, Wuerslin C, Bammer R. Extended hybrid-space SENSE for EPI: off-resonance and eddy current corrected joint interleaved blip-up/down reconstruction. *Neuroimage*. 2017;153:97-108.

17. Hu Y, Ikeda DM, Pittman SM, et al. Multishot diffusion-weighted MRI of the breast with multiplexed sensitivity encoding (MUSE) and shot locally low-rank (shot-LLR) reconstructions. *J Magn Reson Imaging*. 2021;53:807-817.

18. Jeong HK, Gore JC, Anderson AW. High-resolution human diffusion tensor imaging using 2-D navigated multishot SENSE EPI at 7 T. *Magn Reson Med*. 2013;69:793-802.

19. Pruessmann KP, Weiger M, Scheidegger MB, Boesiger P. SENSE: sensitivity encoding for fast MRI. *Magn Reson Med*. 1999;42:952-962.

20. Kellman P, Epstein FH, McVeigh ER. Adaptive sensitivity encoding incorporating temporal filtering (TSENSE). *Magn Reson Med*. 2001;45:846-852.

21. Lin FH, Kwong KK, Belliveau JW, Wald LL. Parallel imaging reconstruction using automatic regularization. *Magn Reson Med*. 2004;51:559-567.

22. Griswold MA, Jakob PM, Heidemann RM, et al. Generalized autocalibrating partially parallel acquisitions (GRAPPA). *Magn Reson Med*. 2002;47:1202-1210.

23. Chen Z, Xia L, Liu F, et al. An improved non-Cartesian partially parallel imaging by exploiting artificial sparsity. *Magn Reson Med*. 2017;78:271-279.

24. Porter DA, Heidemann RM. High resolution diffusion-weighted imaging using readout-segmented echo-planar imaging, parallel imaging and a two-dimensional navigator-based reacquisition. *Magn Reson Med*. 2009;62:468-475.

25. Haldar JP. Low-rank modeling of local k-space neighborhoods (LORAKS) for constrained MRI. *IEEE Trans Med Imaging*. 2014;33:668-681.

26. Jenkinson M, Beckmann CF, Behrens TEJ, Woolrich MW, Smith SM. FSL. *Neuroimage*. 2012;62:782-790.

27. Zhu K, Dougherty RF, Wu H, et al. Hybrid-space SENSE reconstruction for simultaneous multi-slice MRI. *IEEE Trans Med Imaging*. 2016;35:1824-1836.

28. Liao C, Bilgic B, Tian Q, et al. Distortion-free, high-isotropic-resolution diffusion MRI with gSlider BUDA-EPI and multicoil dynamic B0 shimming. *Magn Reson Med*. 2021;86:791-803.

29. Cho J, Berman AJL, Gagoski B, et al. VUDU: motion-robust, distortion-free multi-shot EPI. In: *Proceedings of ISMRM & SMRT Virtual Conference & Exhibition*. Online Conference; 2021. p. 0002. https://martinos.org/~berkin/vudu.pdf

30. So S, Park HW, Kim B, et al. BUDA-MESMERISE: rapid acquisition and unsupervised parameter estimation for T1, T2, M0, B0 and B1 maps. *Magn Reson Med*. 2022;88:292-308.

31. Poser BA, Koopmans PJ, Witzel T, Wald LL, Barth M. Three dimensional echo-planar imaging at 7 tesla. *Neuroimage*. 2010;51:261-266.

32. Bilgic B, Poser B, Langkammer C, Setsompop K, Liao C. 3D-BUDA enables rapid distortion-free QSM acquisition. In: *Proceedings of ISMRM & SMRT Virtual Conference & Exhibition*. Online Conference; 2020. p. 0596.

33. Chen Z, Liao C, Cao X, et al. 3D-CAIPI-BUDA and joint Hankel low-rank reconstruction enable rapid and distortion-free high-resolution T2 * mapping and QSM. *In: Proceedings of the Joint Annual Meeting ISMRM-ESMRMB, London, United Kindom*; 2022. p. 3446. https://archive.ismrm.org/2022/3446.html

34. Nencka A, Hahn A, Rowe D. The use of three navigator echoes in Cartesian EPI reconstruction reduces Nyquist ghosting. *In: Proceedings of the 16th Annual Meeting of ISMRM, Toronto, Canada*; 2008. p. 3032.

35. David A, Feinberg KO. Phase errors in multi-shot echo planar imaging. *Magn Reson Med*. 1994;32:535-539.

36. Breuer FA, Blaimer M, Heidemann RM, Mueller MF, Griswold MA, Jakob PM. Controlled aliasing in parallel imaging results in higher acceleration (CAIPIRINHA) for multi-slice imaging. *Magn Reson Med*. 2005;53:684-691.

37. Breuer FA, Blaimer M, Mueller MF, et al. Controlled aliasing in volumetric parallel imaging (2D CAIPIRINHA). *Magn Reson Med*. 2006;55:549-556.

38. Setsompop K, Gagoski BA, Polimeni JR, Witzel T, Wedeen VJ, Wald LL. Blipped-controlled aliasing in parallel imaging for simultaneous multislice echo planar imaging with reduced g-factor penalty. *Magn Reson Med*. 2012;67:1210-1224.

39. Uecker M, Lai P, Murphy MJ, et al. ESPIRiT - an eigenvalue approach to autocalibrating parallel MRI: where SENSE meets GRAPPA. *Magn Reson Med*. 2014;71:990-1001.

40. Barral JK, Gudmundson E, Stikov N, Etezadi-Amoli M, Stoica P, Nishimura DG. A robust methodology for in vivo T1 mapping. *Magn Reson Med*. 2010;64:1057-1067.

41. Wang Z, Bovik AC, Sheikh HR, Simoncelli EP. Image quality assessment: from error visibility to structural similarity. *IEEE Trans Image Process*. 2004;13:600-612.

42. ALTMAN DG, BLAND JM. Measurement in medicine: the analysis of method comparison studies. *Stat*. 1983;32:307-317.

43. Kraff O, Quick HH. 7T: physics, safety, and potential clinical applications. *J Magn Reson Imaging*. 2017;46:1573-1589.

44. Gruber B, Froeling M, Leiner T, Klomp DWJ. RF coils: a practical guide for nonphysicists. *J Magn Reson Imaging*. 2018;48:590-604.

45. Panych LP, Madore B. The physics of MRI safety. *J Magn Reson Imaging*. 2018;47:28-43.

46. Hendriks AD, D'Agata F, Raimondo L, et al. Pushing functional MRI spatial and temporal resolution further: high-density

receive arrays combined with shot-selective 2D CAIPIRINHA for 3D echo-planar imaging at 7 T. *NMR Biomed*. 2020;33:e4281.

47. Stirnberg R, Stöcker T. Segmented K-space blipped-controlled aliasing in parallel imaging for high spatiotemporal resolution EPI. *Magn Reson Med*. 2021;85:1540-1551.

48. Wang D, Ehses P, Stöcker T, Stirnberg R. Reproducibility of rapid multi-parameter mapping at 3T and 7T with highly segmented and accelerated 3D-EPI. *Magn Reson Med*. 2022;88:2217-2232.

49. Liao C, Manhard MK, Bilgic B, et al. Phase-matched virtual coil reconstruction for highly accelerated diffusion echo-planar imaging. *Neuroimage*. 2019;194:291-302.

50. Wang H, Jia S, Chang Y, et al. Improving GRAPPA reconstruction using joint nonlinear kernel mapped and phase conjugated virtual coils. *Phys Med Biol*. 2019;64:14NT01.

51. Chen Z, Kang L, Xia L, et al. Technical note: sequential combination of parallel imaging and dynamic artificial sparsity framework for rapid free-breathing golden-angle radial dynamic MRI: K-T ARTS-GROWL. *Med Phys*. 2018;45:202-213.

52. Zhang J, Chu Y, Ding W, et al. HF-SENSE: an improved partially parallel imaging using a high-pass filter. *BMC Med Imaging*. 2019;19:1-10.

53. Bilgic B, Chatnuntawech I, Manhard MK, et al. Highly accelerated multishot echo planar imaging through synergistic machine learning and joint reconstruction. *Magn Reson Med*. 2019;82:1343-1358.

54. Akçakaya M, Moeller S, Weingärtner S, Uğurbil K. Scan-specific robust artificial-neural-networks for k-space interpolation (RAKI) reconstruction: database-free deep learning for fast imaging. *Magn Reson Med*. 2019;81:439-453.

55. Hammernik K, Klatzer T, Kobler E, et al. Learning a variational network for reconstruction of accelerated MRI data. *Magn Reson Med*. 2018;79:3055-3071.

56. Tian Q, Zaretskaya N, Fan Q, et al. Improved cortical surface reconstruction using sub-millimeter resolution MPRAGE by image denoising. *Neuroimage*. 2021;233:117946.

57. Aggarwal HK, Mani MP, Jacob M. Modl-mussels: model-based deep learning for multishot sensitivity-encoded diffusion mri. *IEEE Trans Med Imaging*. 2020;39:1268-1277.

58. Kim TH, Cho J, Zhao B, Bilgic B. Accelerated MR parameter mapping with scan-speci c unsupervised networks. In: *Proceedings of the Joint Annual Meeting ISMRM-ESMRMB, London, United Kindom*; 2022. p. 4402. https://archive.ismrm.org/2022/4402.html

59. Yarach U, Chatnuntawech I, Liao C, et al. Rapid reconstruction of blip up-down circular EPI (BUDA-cEPI) for distortion-free dMRI using an unrolled network with U-net as priors. In: *Proceedings of the Joint Annual Meeting ISMRM-ESMRMB, London, United Kindom*; 2022. p. 4348. https://archive.ismrm.org/2022/4348.html

SUPPORTING INFORMATION

Additional supporting information may be found in the online version of the article at the publisher's website.

Figure S1. The flow chart of standard 3D-BUDA image reconstruction.

Figure S2. The phase images of 3D-BUDA image reconstruction for the two-shot GRE-EPI BUDA dataset from a 3T scanner.

Figure S3. Comparison of different reconstructions (SENSE, TOPUP, Hybrid-space SENSE, and 3D-BUDA) on image quality and distortion-correction effect for the same two-shot GRE-EPI BUDA dataset from the 7T Magnetom scanner. First column: Blip-up EPI SENSE results. Second column: Blip-down EPI SENSE results. Third column: TOPUP results. Fourth column: Hybrid-space SENSE results. Last column: The 3D-BUDA image reconstruction results. Three rows are the three planes of 3D imaging. In this dataset, $R_{inplane} \times R_z = 5 \times 1$. The total acquisition time of blip-up EPI, blip-down EPI, TOPUP, Hybrid-space SENSE and 3D-BUDA are 9, 9, 16, 16, and 16 s, respectively. A 2-s FOV-matched FLASH low-resolution pre-scan for coil sensitivity map is counted in these acquisitions.

Figure S4. Comparison of field maps and error maps of different time-matched acquisition schemes ($R_{inplane} = 8$). (a) Reference field map generated by fully-sampled 3D-BUDA data. (b) Field map from four-shot $R_z = 1$ 3D-BUDA data (two blip-up shots and two blip-down shots). (c) Field map from eight-shot $R_z = 2$ 3D-BUDA data (four blip-up shots and four blip-down shots). (d): Corresponding error map of (b). (e): Corresponding error map of (c).